Badger, M. P. S., Schmidt, D. N., Mackensen, A., & Pancost, R. D. (2013). High resolution alkenone palaeobarometry indicates relatively stable pCO_2 during the Pliocene (3.3 to 2.8 Ma). *Philosophical Transactions of the Royal Society A: Mathematical, Physical and Engineering Sciences*, *371*(2001), 20130094. [20130094]. https://doi.org/10.1098/rsta.2013.0094

High resolution alkenone palaeobarometry indicates relatively stable pCO_2 during the Pliocene (3.3 to 2.8 Ma)

Marcus P.S. Badger[1,2], Daniela N. Schmidt[2], Andreas Mackensen[3] and Richard D. Pancost[1]

[1]*Organic Geochemistry Unit, The Cabot Institute and Bristol Biogeochemistry Research Centre, School of Chemistry, University of Bristol, Cantock's Close, Bristol, BS8 1TS, U.K.*

[2]*School of Earth Sciences, Bristol University, Wills Memorial Building, Queens Rd, Bristol, BS8 1RJ, U.K.*

[3]*Alfred Wegener Institute for Polar and Marine Research, Am Alten Hafen 26, 27568 Bremerhaven, Germany.*

Abstract

Temperature reconstructions indicate that the Pliocene was ~ 3 °C warmer globally than today, and several recent reconstructions of Pliocene atmospheric CO_2 indicate that it was above pre-industrial levels and similar to those likely to be seen this century. However, many of these reconstructions have been of relatively low temporal resolution, meaning that these records may have failed to capture variations associated with the 41 Kyr glacial-interglacial cycles thought to operate in the Pliocene. Here we present a new, high temporal resolution alkenone carbon isotope based record of

pCO_2 spanning 2.8 to 3.3 million years ago from ODP Site 999. Our record is of high enough resolution (~19 Kyrs) to resolve glacial-interglacial changes beyond the intrinsic uncertainty of the proxy method. The record suggests that Pliocene CO_2 levels were relatively stable, exhibiting variation less than 55 ppm. We perform sensitivity studies to investigate the possible effect of changing sea surface temperature, which highlights the importance of accurate and precise SST reconstructions for alkenone palaeobarometry, but demonstrate that these uncertainties do not affect our conclusions of relatively stable pCO_2 levels during this interval.

Keywords: *Pliocene, pCO_2, atmospheric carbon dioxide, climate, alkenone, ODP Site 999.*

Introduction

The Pliocene was the most recent epoch in Earth history that had global temperatures greater than today; this, coupled with the similar continental positions and vegetation cover to the present has led to interest in the Pliocene as a possible analogue for the warmth expected by the end of the century [1]. Research to constrain the global temperatures of the Pliocene has been ongoing for some time, including the significant contributions of the PRISM project and successors (e.g. [2-4]), with the consensus that the Pliocene was globally ~ 3 °C warmer than today. Similarly, many studies suggest that Pliocene pCO_2 was also higher than pre-industrial levels [5-8].

Despite these similarities, a significant difference between the Pliocene and the present day is the magnitude and pacing of Pliocene glacial-interglacial changes. Based on the foraminiferal carbonate $\delta^{18}O$ record [9], Pliocene glacial-interglacial cycles were less pronounced than those of the late Quaternary, and they were 41 Kyrs long in contrast to the 100 Kyr cycles of the last 0.7 Ma. Variations in pCO_2 greater than the ~100 ppm fluctuations of the Pleistocene are, therefore, unexpected in a Pliocene world, especially if, as suggested by Pagani et al. [6], Pliocene Earth-system sensitivity was probably greater that 3 °C for a CO_2 doubling. Consistent with this, alkenone-based pCO_2 reconstructions have shown very little glacial-interglacial variation, especially prior to the intensification of northern hemisphere glaciation at 2.8 Ma. These records have been, in part, confirmed by boron isotope based reconstructions [7]. However, due to their low temporal resolution it is possible that they fail to capture higher frequency variability in pCO_2 and represent neither the mean state of the climate system nor its variability on glacial timescales well. A recent reconstruction using boron isotopes [8] has increased the temporal resolution, and in fact targeted specific glacial and interglacial peaks and troughs to attempt to resolve this. Their record exhibits fluctuations in Pliocene pCO_2 that are in fact larger (almost one and a half times) than those observed in Pleistocene ice core records [10-12].

To address this apparent discrepancy, we reconstruct pCO_2 at similarly high resolution from 3.3 to 2.8 Ma using alkenone $\delta^{13}C$ values. We apply our approach to ODP Site 999 in the Caribbean because that is the same site used by Bartoli et al. [8] and Seki et al. [7], allowing direct comparison of our records. Additionally, we also conduct a sensitivity analysis of our reconstructed pCO_2 levels, allowing us to constrain their potential range during this time.

Approach and Methods

Alkenone palaeobarometry

The isotopic fractionation between dissolved inorganic carbon and marine organic matter during photosynthesis (ε_p) is controlled by, amongst other factors, the concentration of CO_2 in the water in which the organism is photosynthesising ($[CO_2]_{aq}$). This is ultimately controlled by the concentration of CO_2 in the overlying atmosphere with which the ocean is in equilibrium. Other factors that can effect ε_p values include physiological factors, such as cell geometry [13] and membrane permeability [14] and environmental factors, such as nutrient and light availability and their impact on carbon demand (i.e. growth rate) and carbon assimilation mechanisms [15-18].

In order to constrain the physiological factors, biomarkers derived from a narrow taxonomic range can be used rather than bulk organic matter. This approach also prevents terrestrial or non-photosynthetically produced organic matter from biasing the marine organic matter isotopic signature [19]. Long chain ketones (alkenones) containing 37 carbons are produced only by a restricted group of haptophyte organisms, such as Gephyrocapsaceae coccolithophores [20]. Thus, work over the past 20 years has focussed specifically on the alkenone palaeobarometer as a tool to reconstruct ancient atmospheric pCO_2, so long as other contributing factors (growth rate, light regime) can be constrained. In order to determine ε_p values, the isotopic composition of both the dissolved inorganic carbon pool (DIC) and organic biomass must be known. The isotopic composition of the organic biomass ($\delta^{13}C_{org}$) is calculated from the alkenone $\delta^{13}C$ ($\delta^{13}C_{37:2}$), corrected for a fractionation between

alkenone and haptophyte biomass by assuming a constant fractionation of 4.2 ‰ (Equation 1; [13, 16]).

Eqn. 1 $$\varepsilon_{alkenone} = \frac{\delta^{13}C_{37:2} + 1000}{\delta^{13}C_{org} + 1000} - 1$$

The isotopic composition of DIC is estimated by measuring the δ^{13}C value of planktic foraminifera, assuming the experimentally determined temperature dependent fractionation between calcite and $CO_{2(g)}$ ($\varepsilon_{calcite\text{-}CO2(g)}$) shown in equation 2 [21]:

Eqn. 2 $$\varepsilon_{calcite\text{-}CO_2(g)} = 11.98 - 0.12T$$

Where T is sea surface temperature (in degrees Celsius). This fractionation factor can then be used to calculate the carbon isotopic composition of $CO_{2(g)}$ ($\delta^{13}C_{CO2(g)}$):

Eqn. 3 $$\delta^{13}C_{CO_2(g)} = \frac{\delta^{13}C_{carbonate} + 1000}{\varepsilon_{calcite\text{-}CO_2(g)} / 1000 + 1} - 1000$$

From this, the carbon isotopic composition of $CO_{2(aq)}$ ($\delta^{13}C_{CO2(aq)}$) can be obtained using the experimentally determined relationship of Mook et al., [22] as shown in equations 4 and 5:

Eqn. 4 $$\varepsilon_{CO_2(aq)\text{-}CO_2(g)} = \frac{-373}{T + 273.15} + 0.19$$

Eqn. 5 $$\delta^{13}C_{CO_2(aq)} = \left(\frac{\varepsilon_{CO_2(aq)\text{-}CO_2(g)}}{1000} + 1 \right) . \left(\delta^{13}C_{CO_2(g)} + 1000 \right) - 1000$$

Photosynthetic fractionation (ε_p) can then be calculated from the determined $\delta^{13}C_{CO2(aq)}$ and $\delta^{13}C_{org}$ (equation 6):

109 Eqn. 6 $$\varepsilon_p = \left(\frac{\delta^{13}C_{CO_2(aq)} + 1000}{\delta^{13}C_{org} + 1000} - 1 \right).1000$$

110 and this is then used to calculate [$CO_{2(aq)}$] according to equation 7:

111 Eqn. 7 $$[CO_{2(aq)}] = \frac{b}{\varepsilon_f - \varepsilon_p}$$

112 where ε_f represents the isotopic fractionation during carbon fixation, assumed here to
113 be constant and 25 ‰ [16]. The '*b*' term represents the summation of physiological
114 factors, such as cell size and growth rate. In the modern ocean this term shows a close
115 correlation with [PO_4^{3-}], allowing estimation of '*b*' by assuming past [PO_4^{3-}] was
116 similar to that present at the site today (0.2 μM; [6, 16, 23]). Finally from [$CO_{2(aq)}$],
117 atmospheric pCO_2 can be calculated, using Henry's law (equation 8) and assuming
118 equilibrium between the surface water and overlying atmosphere:

119 Eqn. 8 $$pCO_2 = \frac{[CO_{2(aq)}]}{K_H}$$

120 The solubility coefficient (K_H) is salinity and temperature dependant, and calculated
121 following the parameterization of Weiss [24, 25]. The assumptions inherent in the
122 above treatment are discussed further below.

123 *Analytical*

124 In this study, analytical determinations of ε_p values were conducted similar to those of
125 previous alkenone paleo-pCO_2 studies (e.g. [6, 7, 23, 26-28]) from ODP Site 999
126 (12°44.639' N, 78°44.360' W, 2838 m water depth. Site 999 is slightly out of
127 equilibrium in the modern ocean, with surface waters oversaturated in CO_2 relative to
128 the atmosphere, providing a small (<10 gCm^2yr^{-1}; [29]) net source of CO_2 to the

129 atmosphere. However the site has been shown to be capable of recording past changes
130 in pCO_2 and the air-sea equilibrium is not thought to have changed significantly from
131 the Pliocene to today (see discussion in [8]). Specifically, 27 samples were freeze
132 dried, ground by hand and solvent extracted either by Soxhlet apparatus or
133 ultrasonically. Soxhlet extractions were performed using a dichloromethane
134 (DCM):methanol (MeOH) azeotrope (2:1, v:v), refluxing for 24 hours. Ultrasonic
135 extractions were performed with, sequentially, DCM, DCM:MeOH (1:1, v:v) and
136 MeOH, repeated 3 times for each solvent with each extraction taking 15 minutes in an
137 ultrasonic bath with ~15 ml of solvent each time. Supernatants were removed and
138 combined before reduction by rotary evaporation and finally evaporated to dryness
139 under a stream of N_2. Following elution through small (4 cm) sodium sulphate
140 columns to remove excess water, total lipid extracts were divided into apolar and
141 polar fractions using alumina flash column chromatography using 4 column volumes
142 of *n*-hexane:DCM (9:1, v:v) and 3 column volumes of MeOH, respectively. Alkenone
143 concentrations were quantified by GC-FID (Hewlett Packard 5890 Series II)
144 following trimethylsilyl derivatisation. The GC oven was programmed to increase in
145 temperature from 70°C to 130°C at 20°Cmin^{-1}, then to 300°C at 4°Cmin^{-1}, finally
146 being held isothermal for 25 min. The column was a CPSil-5CB
147 (dimethylpolysiloxane equivalent), 0.12 μm film thickness, ~50 m length and 0.32
148 mm interdal diameter with a H_2 carrier gas. Alkenone identification was confirmed by
149 GC-MS (ThermoQuest Trace MS, He carrier gas). Absolute compound concentrations
150 were quantified by reference to an internal standard (hexadecan-2-ol) added prior to
151 column chromatography.

152 Sea surface temperature (SST) was reconstructed using the alkenone unsaturation
153 index ($U_{37}^{K'}$;[30, 31]; equation 9):

Eqn. 9 $$U_{37}^{K'} = [C_{37:2}]/[C_{37:2} + C_{37:3}]$$

Where $C_{37:2}$ is the di-unsaturated methyl alkenone and $C_{37:3}$ is the tri-unsaturated compound. SSTs were then calculated using the calibration of Müller et al. [32] (equation 10):

Eqn. 10 $$U_{37}^{K'} = 0.033T + 0.044$$

Concerns have been raised about the use of $U_{37}^{K'}$ as the index approaches 1 [33]. This would be of particular concern at Site 999 as over the studied interval $U_{37}^{K'}$ is > 0.9. However the challenge of calibrating SSTs towards the upper limit of $U_{37}^{K'}$ seems to be a problem largely restricted to sediment trap based calibrations. For core tops a linear calibration seems to hold true, and in fact the updated core-top calibration of Conte et al., [33] is essentially identical to that of Muller et al., [32] (which is more widely used and therefore our preferred). They are especially similar towards the top end of the scale. As we are dealing here with alkenones which have made it to the sea floor a core top calibration seems most appropriate.

Alkenone isotope analyses were performed on a ThermoFisher Delta V connected via a GC isolink and conflo IV to a Trace GC. The GC oven was programmed to increase in temperature from 70°C to 200°C at 20°Cmin^{-1} then to 300°C at 6°Cmin^{-1} and finally held isothermal for 25 min. Conversion to the VPDB scale was calculated by reference to a laboratory standard gas tank of known δ^{13}C. Instrument performance was monitored using an in house fatty acid methyl ester standard and long term precision is ~0.3 ‰.

Ten to fifteen specimens of the planktic foraminifera *Globigerinoides ruber* were picked from the 300-350 μm fraction for $\delta^{13}C$ analysis. This was determined with a Finnigan MAT 251 with an online automatic carbonate preparation device at the Alfred Wegener Institute for Polar and Marine Research, Bremerhaven. Calibration to the VPDB scale was performed using the international NBS19 standard. Reproducibility is better than ±0.06 ‰ over a one-year period based on repeat measurements of a laboratory standard.

The age model for ODP Site 999 is as discussed in Seki et al. [7]. Uncertainty propagation on our alkenone-derived CO_2 estimates was performed by Monte Carlo modelling (n=25000). Uncertainties of 2 °C and 0.1 ‰ were applied to temperature and foraminiferal calcite $\delta^{13}C$, (normal probability function (pdf), 2 σ error) and 2 and 0.1 to salinity and $[PO_4^{3-}]$, respectively (2 σ; uniform pdf). 2 σ errors on alkenone $\delta^{13}C$ were estimated from replicate runs, calcite $\delta^{13}C$ from repeat runs of an internal standard, estimated integrated analytical and calibration error for $U_{37}^{K'}$ based temperatures [32] and conservative estimates of likely variation for salinity and $[PO_4^{3-}]$. An 11 % error on the slope of $b=a[PO_4]+c$ was assumed [26].

Results

Alkenone and *G. ruber* $\delta^{13}C$ values (Figure 1b) were used to calculate ε_p values (Figure 1a). These ε_p values are fairly stable throughout the study interval, varying between 12.2 and 9.4 ‰. This is close to the values reported by Seki et al., [7] for the same Site over this interval (12.2 - 10.9 ‰).

Using modern $[PO_4^{3-}]$ for the Caribbean Sea, ε_p values can be converted to $[CO_2]_{(aq)}$ (Equation 7; Figure 1b). Using our SSTs derived from $U_{37}^{K'}$ indices and assuming air-

198 sea equilibrium, $[CO_2]_{(aq)}$ can then be used to determine atmospheric pCO_2 (Equation
199 8). $U_{37}^{K'}$ indices range from 0.90 to 0.99 (close to the maximum recordable value for
200 $U_{37}^{K'}$), resulting in SSTs at Site 999 of ~28 °C that show a slight decrease over the 500
201 Kyrs of our record (Figure 2b). These are ~ 2 °C higher than the planktic foraminifer
202 (*Globigerinoides sacculifer)* Mg/Ca based SST record of Groeneveld [34] from the
203 same site, < 1 °C lower than the SSTs estimated by Bartoli et al. [8] based on a
204 seawater Mg/Ca correction of these same data, and very similar to modern SSTs that
205 range from 26.7 °C to 28.2 °C [35].

206 Our resulting pCO_2 reconstruction (Figure 2a) reveals relatively stable pCO_2 values
207 that are within the range of previously published alkenone records from ODP Site 999
208 (without the lith size correction of Seki et al. [7]) and elsewhere [6]. All of our
209 reconstructed pCO_2 (250-300 ppm) levels are similar to or slightly higher than the
210 240-290 ppm for Pleistocene interglacials reconstructed from ice cores [10-12] and
211 are consistent with glacial-interglacial variability of at most 40 ppm. In fact, the entire
212 range of determined pCO_2 values for the end of the Pliocene is less than the 80 ppm
213 difference between the Holocene and the Last Glacial Maximum [36]. There is some
214 variability outside of uncertainty in the ε_p record in the younger part of the record,
215 hinting to some variability after 3 Ma, however once the full propagation of
216 uncertainties are taken through to the CO_2 reconstruction, the variation is no longer
217 significant. Below, we discuss the pCO_2 estimates, their variations with respect to
218 Pliocene glacial-interglacial cycles and the potential range of pCO_2 given our
219 assumptions of growth rate and SST.

220

221 **Discussion**

222 *Glacial-Interglacial* pCO_2 *variations*

223 We estimate absolute pCO_2 to be around ~270 ppm for much of the period studied
224 here, based on our most likely temperature, cell geometry and growth rates
225 assumptions (see subsequent sections for sensitivity analysis of these parameters).
226 This is similar to pre-industrial levels, and around the peak level of the Pleistocene ice
227 core records (298.6 ppm; [10-12]). Our record is within the range of estimates given
228 by Pagani et al., [6] (Figure 3a), although it should be noted that these authors report a
229 broad range of absolute CO_2 due to differences between the sites. Our record is below
230 the 'CO_{2slope}' reported in Pagani et al. [6] i.e. their extrapolated trend from the early
231 Pliocene to the present day.

232 Estimating absolute pCO_2 from a single site is complicated by uncertainty as to
233 whether the site has been in equilibrium with the atmosphere over the period of
234 interest. As highlighted by Pagani et al. [6], different sites can exhibit very different
235 estimates for atmospheric pCO_2, as not all of the surface ocean is in equilibrium with
236 the atmosphere [29]. The surface ocean at Site 999 is close to equilibrium today [29]
237 and reconstructed alkenone based pCO_2 values are similar to ice core records where
238 they overlap in the Pleistocene [7] suggesting that the site was in equilibrium through
239 much of this time. It is difficult to know whether this remained so in the Pliocene with
240 different circulation in the Caribbean, so as with all single site records, our absolute
241 pCO_2 should be treated with some care.

242 Our absolute pCO_2 is similar to the alkenone-based record without secondary
243 corrections of Seki et al. [7] from the same site, although somewhat lower than both
244 the cell size corrected alkenone record and boron isotope based records of Seki et al.
245 [7] (Figure 3a). Bartoli et al. [8] report a broad range of pCO_2 (170-400 ppm; Figure

246 3b) and our record is within that range. The difference between our record and the
247 cell size corrected record of Seki et al. [7] (Figure 4) highlights the importance of
248 secondary corrections, particularly on alkenone based method and we explore this
249 further below. Given the potential difficulty of assessing absolute pCO_2 levels from
250 single site records we now focus on pCO_2 variability during this interval in the
251 Pliocene.

252 Previous alkenone-based palaeobarometry has been at a relatively low temporal
253 resolution, and given the 41 kyr glacial-interglacial variability in the Pliocene world,
254 it is possible that these records do not capture rapid changes in pCO_2 [6, 7]. Our new
255 record increases the resolution of the alkenone-based records, but unlike the boron
256 record of Bartioli et al. [8] shows virtually invariant pCO_2 within the precision of the
257 alkenone palaeobarometer (Figure 4). The differences between these two records
258 cannot be due to differences in ocean-atmosphere equilibrium, as both are based on
259 Site 999. The magnitude of variability in our record is similar to that seen in previous,
260 low resolution records (i.e. the boron and alkenone records of Seki et al. [7], and the
261 alkenone records of Pagani et al. [6]) which may suggest that these records have
262 captured pCO_2 variability despite their lower resolution, and the small estimated range
263 of Pliocene pCO_2 is a feature of Pliocene climate dynamics rather than a sampling
264 artefact. An alternative hypothesis is that the alkenone palaeobarometer
265 underestimates variability for an as yet unknown reason.

266 It should perhaps not be surprising that Pliocene pCO_2 appears to be relatively stable;
267 the large, 100 Kyr glacial-interglacial cycles of the Pleistocene are associated with ~
268 100 ppm of change in pCO_2 [10-12], and it is likely that the smaller amplitude
269 variations in the Pliocene would be associated with significantly smaller pCO_2

changes. The large amplitude changes of Bartoli et al. [8] are therefore somewhat surprising. Given that the full uncertainty envelope for our alkenone pCO_2 records is approximately ±40 ppm, it is plausible that smaller, Pliocene variations in pCO_2 would be below the detection limit of our methods.

Cell size and productivity corrections

Atmospheric pCO_2 reconstructions from alkenone isotopes can be affected by cell size and productivity, i.e growth rate variations. Seki et al. [7] applied a conceptual cell size correction to the alkenone data from Site 999, based on the low resolution lith size record of Kameo and Bralower [37]. However, recent high resolution data shows no evidence of changes in coccolith size over the time interval of interest [38]. Crucially, there are no changes in coccolith size – and thus, inferred coccolithophorid cell size – on glacial-interglacial timescales, and hence it is unlikely that they could account for the low variability observed here. It remains possible, however, that they could account for the relatively low absolute pCO_2 values determined for the Pliocene at Site 999, compared to δ^{11}B-based estimates (~400 ppm; [7, 8]).

There is not yet a consensus approach to the application of a cell geometry correction (see discussion in Seki et al. [7] and Henderiks and Pagani [39]), however attempts have been made to correct for cell size changes by adjusting the '*b*' term in equation 7. Hendericks and Pagani [39] adjusted the '*b*' term based on the ratio of "fossil" haptophyte cell volume:surface area ($V{:}SA_{fossil}$) to that of the modern *Emiliania huxleyi* ($V{:}SA_{E.hux}$) used for modern culture studies. (equation 11).

292 Eqn. 11 $$b' = b.\left[\frac{V:SA_{fossil}}{V:SA_{E.hux}}\right]$$

293 Popp et al., 1998 determined $V:SA_{E.hux}$ to be 0.9 ± 0.1μm and the value of $V:SA_{fossil}$
294 can be estimated using the relationship between cell diameter (D_{cell}) and
295 *Reticulofenestra* coccolith length ($L_{coccolith}$; [39]; equation 12):

296 Eqn. 12 $$D_{cell} = 0.55 + 0.88.L_{coccolith}$$

297 Reticulofenestrids (Noelaerhabdaceae) are thought to be important alkenone
298 producers in the past [39], although there is some evidence that this may not be the
299 case for some earlier parts of the Neogene [40].

300 The cell size correction results in a linear correction to pCO_2, the gradient of which is
301 temperature dependent (Figure 5), where a larger coccolith length results in higher
302 reconstructed CO_2. This effect is increased at higher SSTs. Approximately 1 μm of
303 change in $L_{coccolith}$ would be required to alter pCO_2 beyond our uncertainty envelope.
304 This represents a size change of ~25 %, and there is no evidence for such a change on
305 glacial-interglacial timescales at Site 999 [38].

306 Similarly, there is no evidence that growth rate changed on glacial-interglacial
307 timescales at Site 999 through the interval studied. Seki et al. [7] noted that there
308 could have been changes in the oceanography of the site as the shoaling of the
309 Panama isthmus isolated the Caribbean from the Pacific. O'Dea et al. [41] had argued
310 that these changes could have influenced the nutrient regime at Site 999; however, the
311 closure of the strait to deep water is thought to have been complete by 4.6 Ma [42].
312 Moreover, alkenone and other biomarker concentrations and mass accumulation rates
313 are low and relatively invariant over the studied interval [7]. Other indicators of

productivity (organic carbon mass accumulation rates) have not shown evidence of significant changes in productivity [43]. We have improved the resolution of these analyses to 16-kyr and no systematic variation is apparent, suggesting that on glacial-interglacial timescales no correction to our pCO_2 reconstruction is justified.

No proxy exists to directly reconstruct the growth rate conditions at the site during the Pliocene. Our approach is to use the relationship between '*b*' and [PO_4^{3-}] which has been calibrated globally [6, 23, 44] and appears to be a proxy for growth limiting nutrients [23]. Our favoured assumption is to use a modern day value for surface water [PO_4^{3-}] at Site 999 [45] but here we explore the possibility that this assumption is incorrect. To this end, we have performed a sensitivity test, and apply a [PO_4^{3-}] which represents an oligotrophic site (0.05 μM), a high nutrient area similar to present day eastern equatorial Pacific (0.6 μM) and an extreme case representative of an active upwelling region (0.9 μM)[45]. The resulting pCO_2 reconstructions vary from ~230 ppm for the oligotrophic model, ~390 ppm for the eastern equatorial pacific model, and ~480 ppm for the extreme case (Figure 6). The sensitivity tests demonstrate that our favoured assumptions that result in pCO_2 of ~ 270 ppm may be a lower bound, and if the nutrient regime was significantly different in the Pliocene then our record may be an underestimate. However, as discussed above, we have no direct evidence for such a change, and critically, no evidence of changes on glacial-interglacial timescales that may explain the low variability of our record.

The importance of accurate and precise temperature determinations

Critical to the validity of alkenone isotope pCO_2 reconstructions is the accurate and precise determination of sea surface temperature. Whilst some of the previously

discussed parameters (such as an evolutionary change in haptophyte cell size, or significant changes in oceanographic regime leading to changes in growth rate) are likely stable over short periods of time, sea surface temperatures can change on glacial-interglacial timescales and affect pCO_2 estimates. SST is involved three times in the reconstruction of pCO_2 from alkenone $\delta^{13}C$ values, in the conversion of $\delta^{13}C_{calcite}$ to $\delta^{13}C_{CO2(g)}$ values (equations 2 - 3), $\delta^{13}C_{CO2(g)}$ to $\delta^{13}C_{CO2(aq)}$ values (equations 4 -5) and the calculation of the solubility coefficient (equation 8). This results in a non-linear temperature dependence of the $\delta^{13}C_{alkenone}$-pCO_2 relationship (Figure 7). The size of this effect can be important both in terms of accuracy and precision of alkenone-based reconstructions. Proxies that show potential to reconstruct SST suitable for alkenone palaeobarometry include those based on alkenone unsaturation indices [30, 31] and planktic foraminiferal Mg/Ca ratios [46]. Estimates of uncertainty in the measurement of SST using either Mg/Ca or alkenone unsaturation suggests a combined analytical and correlation error of approximately 2 °C (2σ; [47, 48]),

The relationships between alkenone $\delta^{13}C$, ε_p, $[CO_2]_{(aq)}$ and pCO_2, and the effects of SST are shown in Figure 7. Higher reconstructed SST results in higher apparent ε_p for a given $\delta^{13}C$ value (Figure 7a) and higher pCO_2 for a given $[CO_2]_{(aq)}$ (Figure 7b). Higher reconstructed SST, therefore, results in higher apparent pCO_2 for a given $\delta^{13}C$ value by integrating these two effects (Figure 7d). The magnitude of this effect is more pronounced at higher pCO_2 and more negative alkenone $\delta^{13}C$ values (Figure 7d), and also as ε_p approaches ε_f (see the discussion in Pagani et al. [27]).

For example, for an alkenone $\delta^{13}C$ value of -25 ‰ (which gives a representative pCO_2 of 300 ppm in this sensitivity test), the 2 °C analytical and calibration error in Mg/Ca

or $U^{K'}_{37}$ SST estimates would result in a error of ~ 23 ppm in pCO_2; at a more negative $\delta^{13}C$ value of -28 ‰ (pCO_2=400 ppm) the same error in SST results in an error of ~34 ppm in pCO_2 (Figure 7d). One result of this is that an incorrect or overestimated decline in SST can lead to an artificial apparent decline in pCO_2. This requires careful consideration if estimating climate or earth system sensitivity from coupled alkenone pCO_2 and SST records. To apply this directly to the data presented here, SSTs 2 °C cooler than our data suggests (ie at the edge of the quoted uncertainty for alkenone unsaturation based temperatures) would result in average reconstructed pCO_2 over the interval studied of 255 ppm, a 15 ppm reduction. Conversely SSTs 2 °C warmer would give average reconstructed pCO_2 20 ppm higher, at 290 ppm.

For the Pliocene, the choice of SST record is important, given the uncertainty as to the possible effects of changing Mg/Ca_{sw} on Mg/Ca palaeothermometry. Recent reconstructions of Pliocene Mg/Ca_{sw} suggest that the Pliocene value could have been more than 1 mol/mol lower [49], which could change the reconstructed SST by as much as 6 °C . Our preferred $U^{K'}_{37}$ temperatures for Site 999 lie between the Mg/Ca_{sw} corrected and uncorrected records for the same time period [8, 34]. The uncorrected SST estimates of Groeneveld [34] are ~ 3.8 °C lower and would result in pCO_2 ~29 ppm lower if applied to our records, whereas the up to 2.5 °C higher temperatures of Bartoli et al. [8] would increase our estimates by ~ 24 ppm. At Site 999 today SSTs vary between 26.7 °C and 28.2 °C whereas temperatures at the habitat depth likely for *G. sacculifer* it is 24.2 – 26.6 °C [35], and so the cooler temperatures of Groeneveld [34] may be due to differences in depths of the recording organism. Crucially however, none of the SST records for Site 999 indicate glacial – interglacial

386 variability that would result in pCO_2 variations with a magnitude similar to those of
387 the Pleistocene, or as recorded by Bartoli et al., [8].

388

389 **Synthesis**

390 We reconstruct atmospheric pCO_2 for the Pliocene (3.3 to 2.8 Ma) of ~270 ±40 ppm
391 (2σ) similar to Pleistocene interglacials. We record little or no variability suggesting
392 pCO_2 was persistently at about Pleistocene interglacial values. Only at the outer
393 bounds of our uncertainty envelope would we record Pleistocene glacial levels of
394 pCO_2. Uncertainty in our assumptions for productivity, SST and cell size all result in
395 a broad uncertainty envelope around our preferred parameterization, with our best
396 estimate suggesting pCO_2 was between ~ 230 and 300 ppm. These absolute values are
397 lower than those derived from other approaches and this could reflect a combination
398 of local paleoceanographic conditions and the impact of secondary effects on
399 alkenone $\delta^{13}C$ values. However, we see no evidence that such secondary effects were
400 varying on glacial-interglacial timescales, and consequently, our data collectively
401 indicate that pCO_2 at this point in the Pliocene was relatively stable. We see no
402 evidence for glacial-interglacial changes larger than the fundamental precision of the
403 proxy method of 40 ppm, and our record supports the idea that minimal pCO_2
404 variability was associated with the small glacial-interglacial climate variability of the
405 Pliocene. However, further work is needed to improve the precision of all proxy
406 methods, and to reconcile differences between records of Pliocene pCO_2.

407

408 **Acknowledgments**

This research used samples and data provided by the Ocean Drilling Program which is sponsored by the U.S. National Science Foundation and participating countries under the management of Joint Oceanic Institutions. We would like to thank Alex Hull, Gemma Bowler and Marilyn Potts for labwork, Lisa Schönborn and Günter Meyer for technical assistance and Alison Kuhl and Ian Bull of the NERC Life Sciences Mass Spectrometry facility for research support. We thank two anonymous reviewers and the editor, Dan Lunt, for careful comments which greatly improved the manuscript. MPSB was funded by NERC grant NE/H006273/1, DNS by a Royal Society URF. RDP acknowledges the Royal Society Wolfson Research Merit Award.

References

1. Solomon, S., et al., *Contribution of Working Group I to the Fourth Assessment Report of the Intergovernmental Panel on Climate Change*2007, Cambridge, U.K. and New York. USA: Cambridge University Press.
2. Dowsett, H., J. Barron, and R. Poore, *Middle Pliocene sea surface temperatures: A global reconstruction.* Marine Micropaleontology, 1996. **27**(1-4): p. 13-25.
3. Dowsett, H.J., *The PRISM palaeoclimate reconstruction and Pliocene sea-surface temperature*. Deep-Time Perspectives on Climate Change: Marrying the Signal from Computer Models and Biological Proxies, ed. M.H.A.M.G.F.J.S.D.N. Williams2007. 459-480.
4. Dowsett, H.J., et al., *Sea surface temperatures of the mid-Piacenzian Warm Period: A comparison of PRISM3 and HadCM3.* Palaeogeography Palaeoclimatology Palaeoecology, 2011. **309**(1-2): p. 83-91.
5. Raymo, M.E., et al., *Mid-Pliocene warmth: Stronger greenhouse and stronger conveyor.* Marine Micropaleontology, 1996. **27**(1-4): p. 313-326.
6. Pagani, M., et al., *High Earth-system climate sensitivity determined from Pliocene carbon dioxide concentrations.* Nature Geoscience, 2010. **3**(1): p. 27-30.
7. Seki, O., et al., *Alkenone and boron-based Pliocene pCO2 records.* Earth and Planetary Science Letters, 2010. **292**(1-2): p. 201-211.
8. Bartoli, G., B. Honisch, and R.E. Zeebe, *Atmospheric CO(2) decline during the Pliocene intensification of Northern Hemisphere glaciations.* Paleoceanography, 2011. **26**.
9. Lisiecki, L.E. and M.E. Raymo, *A Pliocene-Pleistocene stack of 57 globally distributed benthic delta O-18 records (vol 20, art no PA1003, 2005).* Paleoceanography, 2005. **20**(2).
10. Siegenthaler, U., et al., *Stable Carbon Cycle¬Climate Relationship During the Late Pleistocene.* Science, 2005. **310**(5752): p. 1313-1317.

11. Petit, J.R., et al., *Climate and atmospheric history of the past 420,000 years from the Vostok ice core, Antarctica.* Nature, 1999. **399**(6735): p. 429-436.
12. Luthi, D., et al., *High-resolution carbon dioxide concentration record 650,000-800,000 years before present.* Nature, 2008. **453**(7193): p. 379-382.
13. Popp, B.N., et al., *Effect of phytoplankton cell geometry on carbon isotopic fractionation.* Geochimica Et Cosmochimica Acta, 1998. **62**(1): p. 69-77.
14. Riebesell, U., et al., *The effects of varying CO2 concentration on lipid composition and carbon isotope fractionation in Emiliania huxleyi.* Geochimica Et Cosmochimica Acta, 2000. **64**(24): p. 4179-4192.
15. Laws, E.A., et al., *Dependence of Phytoplankton Carbon Isotopic Composition on Growth-Rate and [Co2](Aq) - Theoretical Considerations and Experimental Results.* Geochimica Et Cosmochimica Acta, 1995. **59**(6): p. 1131-1138.
16. Bidigare, R.R., et al., *Consistent fractionation of C-13 in nature and in the laboratory: Growth-rate effects in some haptophyte algae.* Global Biogeochemical Cycles, 1997. **11**(2): p. 279-292.
17. Laws, E.A., R.R. Bidigare, and B.N. Popp, *Effect of growth rate and CO(2) concentration on carbon isotopic fractionation by the marine diatom Phaeodactylum tricornutum.* Limnology and Oceanography, 1997. **42**(7): p. 1552-1560.
18. Bidigare, R.R., et al., *Iron-stimulated changes in C-13 fractionation and export by equatorial Pacific phytoplankton: Toward a paleogrowth rate proxy.* Paleoceanography, 1999. **14**(5): p. 589-595.
19. Hayes, J.M., et al., *Compound-Specific Isotopic Analyses - a Novel Tool for Reconstruction of Ancient Biogeochemical Processes.* Organic Geochemistry, 1990. **16**(4-6): p. 1115-1128.
20. Marlowe, I.T., et al., *Long-Chain Alkenones and Alkyl Alkenoates and the Fossil Coccolith Record of Marine-Sediments.* Chemical Geology, 1990. **88**(3-4): p. 349-375.
21. Romanek, C.S., E.L. Grossman, and J.W. Morse, *Carbon Isotopic Fractionation in Synthetic Aragonite and Calcite - Effects of Temperature and Precipitation Rate.* Geochimica Et Cosmochimica Acta, 1992. **56**(1): p. 419-430.
22. Mook, W.G., Bommerso.Jc, and Staverma.Wh, *Carbon Isotope Fractionation between Dissolved Bicarbonate and Gaseous Carbon-Dioxide.* Earth and Planetary Science Letters, 1974. **22**(2): p. 169-176.
23. Pagani, M., et al., *Marked decline in atmospheric carbon dioxide concentrations during the Paleogene.* Science, 2005. **309**(5734): p. 600-603.
24. Weiss, R.F., *The solubility of nitrogen, oxygen and argon in water and seawater.* Deep Sea Research and Oceanographic Abstracts, 1970. **17**(4): p. 721-735.
25. Weiss, R.F., *Carbon dioxide in water and seawater: the solubility of a non-ideal gas.* Marine Chemistry, 1974. **2**(3): p. 203-215.
26. Pagani, M., M.A. Arthur, and K.H. Freeman, *Miocene evolution of atmospheric carbon dioxide.* Paleoceanography, 1999. **14**(3): p. 273-292.
27. Pagani, M., et al., *The Role of Carbon Dioxide During the Onset of Antarctic Glaciation.* Science, 2011. **334**(6060): p. 1261-1264.
28. Bijl, P.K., et al., *Transient Middle Eocene Atmospheric CO(2) and Temperature Variations.* Science, 2010. **330**(6005): p. 819-821.

29. Takahashi, T., et al., *Climatological mean and decadal change in surface ocean pCO(2), and net sea-air CO2 flux over the global oceans (vol 56, pg 554, 2009).* Deep-Sea Research Part I-Oceanographic Research Papers, 2009. **56**(11): p. 2075-2076.
30. Brassell, S.C., et al., *Molecular Stratigraphy - a New Tool for Climatic Assessment.* Nature, 1986. **320**(6058): p. 129-133.
31. Prahl, F.G. and S.G. Wakeham, *Calibration of Unsaturation Patterns in Long-Chain Ketone Compositions for Paleotemperature Assessment.* Nature, 1987. **330**(6146): p. 367-369.
32. Muller, P.J., et al., *Calibration of the alkenone paleotemperature index U-37(K ') based on core-tops from the eastern South Atlantic and the global ocean (60 degrees N-60 degrees S).* Geochimica Et Cosmochimica Acta, 1998. **62**(10): p. 1757-1772.
33. Conte, M.H., et al., *Global temperature calibration of the alkenone unsaturation index (U(37)(K ')) in surface waters and comparison with surface sediments.* Geochemistry Geophysics Geosystems, 2006. **7**.
34. Groeneveld, J., *Effect of the Pliocene closure of the Panamanian Gateway on Caribbean and east Pacific sea surface temperatures and salinities by applying combined Mg/Ca and δ18O measurements (5.6-2.2Ma)*, 2005, University of Kiel: Kiel. p. 165.
35. Locarnini, R.A., et al., *World Ocean Atlas 2009, Volume 1: Temperature*. NOAA Atlas NESDIS 68, ed. S. Levitus2010, Washington, D.C.: U.S Government Printing Office.
36. Barnola, J.M., et al., *Vostok ice core provides 160,000-year record of atmospheric CO2.* Nature, 1987. **329**(6138): p. 408-414.
37. Kameo, K. and T.J. Bralower, *Neogene calcareous nannofossil biostratigraphy of Site 998, 999 and 1000, Caribbean Sea*, in *Proceedings of the Ocean Drillin Program, Scientific Results*, R.M. Leckie, et al., Editors. 2000, Ocean Drilling Program: College Station, TX. p. 3-17.
38. Herrmann, S. and H.R. Thierstein, *Cenozoic coccolith size changes-Evolutionary and/or ecological controls?* Palaeogeography Palaeoclimatology Palaeoecology, 2012. **333**: p. 92-106.
39. Henderiks, J. and M. Pagani, *Refining ancient carbon dioxide estimates: Significance of coccolithophore cell size for alkenone-based pCO(2) records.* Paleoceanography, 2007. **22**(3).
40. Plancq, J., et al., *Alkenone producers during late Oligocene-early Miocene revisited.* Paleoceanography, 2012. **27**.
41. O'dea, A., et al., *Environmental change preceded Caribbean extinction by 2 million years.* Proceedings of the National Academy of Sciences of the United States of America, 2007. **104**(13): p. 5501-5506.
42. Haug, G.H. and R. Tiedemann, *Effect of the formation of the Isthmus of Panama on Atlantic Ocean thermohaline circulation.* Nature, 1998. **393**(6686): p. 673-676.
43. Party, S.S., *Site 999*, in *Proceeding of the Ocean Drilling Program. Initial Reports*, R. Haraldur Sigurdsson, et al., Editors. 1997, Ocean Drilling Program: College Station, TX. p. 131-230.
44. Laws, E.A., et al., *Controls on the molecular distribution and carbon isotopic composition of alkenones in certain haptophyte algae.* Geochemistry Geophysics Geosystems, 2001. **2**.

45. Garcia, H.E., et al., *World Ocean Atlas 2009, Volume 4: Nutrients (phosphate, nitrate, silicate)*. NOAA Atlas NESDIS 71, ed. S. Levitus2010, Washington, D.C.: U.S Government Printing Office.
46. Nurnberg, D., J. Bijma, and C. Hemleben, *Assessing the reliability of magnesium in foraminiferal calcite as a proxy for water mass temperatures.* Geochimica Et Cosmochimica Acta, 1996. **60**(5): p. 803-814.
47. Dekens, P.S., et al., *A 5 million year comparison of Mg/Ca and alkenone paleothermometers.* Geochemistry Geophysics Geosystems, 2008. **9**.
48. Anand, P., H. Elderfield, and M.H. Conte, *Calibration of Mg/Ca thermometry in planktonic foraminifera from a sediment trap time series.* Paleoceanography, 2003. **18**(2).
49. Fantle, M.S. and D.J. DePaolo, *Sr isotopes and pore fluid chemistry in carbonate sediment of the Ontong Java Plateau: Calcite recrystallization rates and evidence for a rapid rise in seawater Mg over the last 10 million years.* Geochimica et Cosmochimica Acta, 2006. **70**(15): p. 3883-3904.
50. Honisch, B., et al., *Atmospheric Carbon Dioxide Concentration Across the Mid-Pleistocene Transition.* Science, 2009. **324**(5934): p. 1551-1554.

564

565 **Figure Captions**

566 **Figure 1a.** ε_p values (filled square symbols and fine black line) are shown with the
567 epibenthic foraminferal oxygen isotope record for the site (Grey/heavy solid line;[42])
568 for comparison. For ε_p the plotted uncertainty envelopes represent maximum and
569 minimum estimates based on 2σ extremes of the $\delta^{13}C_{37:2}$ measurement (dashed line)
570 and a full monte carlo propagation of associated uncertainties (dotted line; see main
571 text for details). **b.** *G. ruber* (open diamonds) and alkenone $\delta^{13}C$ values (filled
572 circles); error bars are 2σ analytical errors based on replicate measurements.

573 **Figure 2a.** pCO_2 reconstruction based on our new high resolution $\delta^{13}C_{37:2}$ records
574 (filled squares and line); as in Figure 1, the dashed line shows an uncertainty envelope
575 representing minimum and maximum estimates based on 2σ extremes of the $\delta^{13}C_{37:2}$
576 measurement (dashed line) and a full monte carlo propagation of associated
577 uncertainties (dotted line; see main text for details). **b.** Sea surface temperature
578 estimates based on the alkenone unsaturation index. Calibration and measurement
579 uncertainties are approximately 2 °C and are omitted for clarity. **c.** Benthic
580 foraminiferal oxygen isotope stack LR04 (Grey/heavy solid line; [9]) for comparison.

581 **Figure 3** Selected records of pCO_2 and climate from the Pliocene to present. **a.**
582 Alkenone-based pCO_2 records from Seki et al. [7] corrected for cell geometry (dashed
583 line; minimum and maximum estimates) and uncorrected (purple filled squares and
584 line; minimum and maximum estimates) and Pagani et al. [6] shown here as their
585 reconstructed 'CO_{2slope}' (from top to bottom: from ODP sites 1012 [khaki heavy line];
586 1208 [green heavy line]; 982 [cyan heavy line]; 1012 with an alternative nutrient
587 scenario [heavy dashed line]; and 806 [lilac heavy line]. Our record is shown as open

588 squares and line with the error envelope from the monte carlo model (see text). **b.**
589 δ^{11}B-based pCO_2 records from Seki et al. [7] calculated using modelled [CO_3^{2-}] (blue
590 filled diamonds) and assuming modern total alkalinity (TA; red filled circles). Error
591 bars are ±25 ppm and the error envelope is based on varying TA by ±5%. The records
592 of Bartoli et al. [8] are shown in grey, (open grey circles and line, with 2σ uncertainty
593 envelope) along with that of Hönisch et al. [50] (filled grey circles and line, , with 2σ
594 uncertainty envelope). Also shown is the Antarctic ice core record of pCO_2 over the
595 last 800 Kyrs for comparison ([12] and references therein). **c.** Benthic foraminiferal
596 oxygen isotope stack LR04 (Grey/heavy solid line; [9]) for comparison (Online
597 version in colour.)

598 **Figure 4** Pliocene pCO_2 records from ODP Site 999. **a** Alkenone-based pCO_2 records
599 from Seki et al. [7] corrected for cell geometry (dashed line; minimum and maximum
600 estimates) and uncorrected (purple filled squares and line; minimum and maximum
601 estimates) and our new higher resolution record (filled squares and line); the dashed
602 line shows an uncertainty envelope representing minimum and maximum estimates
603 based on 2σ extremes of the $\delta^{13}C_{37:2}$ measurement (dashed line) and a full monte carlo
604 propagation of associated uncertainties (dotted line; see main text for details). **b** δ^{11}B-
605 based pCO_2 records from Seki et al. [7] calculated using modelled [CO_3^{2-}] (blue filled
606 diamonds) and assuming modern total alkalinity (TA; red filled circles). Error bars are
607 ±25 ppm and the error envelope is based on varying TA by ±5%. The record of
608 Bartoli et al. [8] is shown as grey open circles and line with 2σ uncertainty envelope
609 (grey lines). **c.** Benthic foraminiferal oxygen isotope stack LR04 (Grey/heavy solid
610 line; [9]) for comparison (Online version in colour.)

Figure 5 The effect of the coccolith length ($L_{coccolith}$) correction on reconstructed pCO_2. Lines represent the correction applied at different sea surface temperatures at 3 °C intervals (as labelled). White circles represent the uncorrected values (where the coccolith length equals that of modern cultured coccolithophores). These were calculated based on representative values of $\delta^{13}C_{37:2}$= -20 ‰ and $\delta^{13}C_{cc}$= 2 ‰, [PO_4^{3-}]=0.25 μM and S=35 psu.

Figure 6 Phosphate concentrations are closely correlated with apparent '*b*' term, most likely due to a linkage to growth rate. Our favoured assumption uses the modern day concentration for the site (0.2 μM; black filled squares and line) with minimum and maximum estimates based on 2 σ extremes of the $\delta^{13}C_{37:2}$ measurement (dashed line) and a full monte carlo propagation of associated uncertainties (which includes a ± 0.1 μM on [PO_4^{3-}]; dotted line; see main text for details). We also include reconstructions with [PO_4^{3-}] representative of an oligotrophic site (0.05 μM; open squares), a high nutrient area similar to the eastern equatorial Pacific (0.6 μM; open triangles) and an extreme case representative of an active upwelling region (0.9 μM; open circles)[45]. The appropriate '*b*' term according to the relationship of Pagani et al. [6] is shown for each reconstruction.

Figure 7 The relationship between ε_p and alkenone $\delta^{13}C$ (**a**); [$CO_{2(aq)}$] and pCO_2 **(b)**; ε_p and pCO_2 **(c)**; and alkenone and $\delta^{13}C$ **(d)** are all affected by SST. Lines are calculated at varied SST at 3 °C intervals (as labelled), and were calculated based on representative starting values of $\delta^{13}C_{37:2}$= -20 ‰; $\delta^{13}C_{cc}$= 2 ‰. [PO_4^{3-}]=0.25 μM, S=35 psu.

Short title: *Stable Pliocene pCO_2*

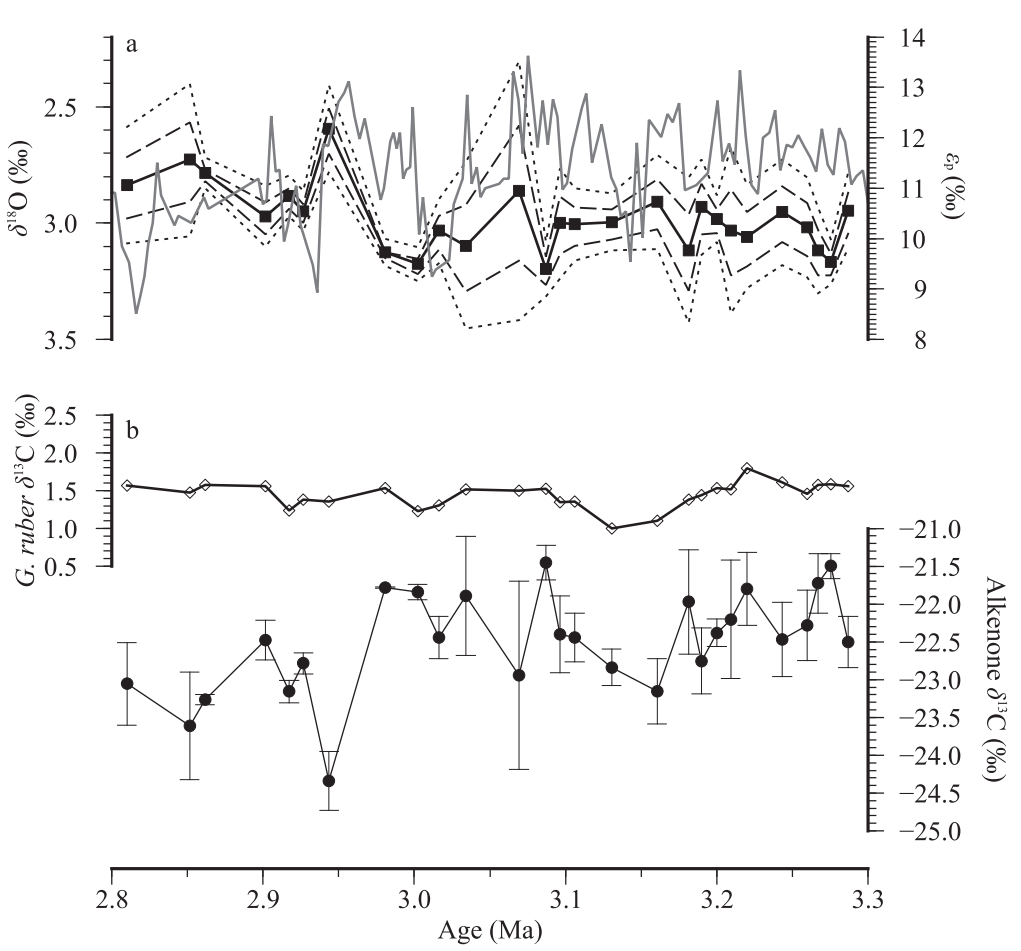

Figure 1a. ε_p values (filled square symbols and fine black line) are shown with the epibenthic foraminferal oxygen isotope record for the site (Grey/heavy solid line;[42]) for comparison. For ε_p the plotted uncertainty envelopes represent maximum and minimum estimates based on 2σ extremes of the $\delta^{13}C_{37:2}$ measurement (dashed line) and a full monte carlo propagation of associated uncertainties (dotted line; see main text for details). **b.** G. ruber (open diamonds) and alkenone δ^{13}C values (filled circles); error bars are 2σ analytical errors based on replicate measurements.

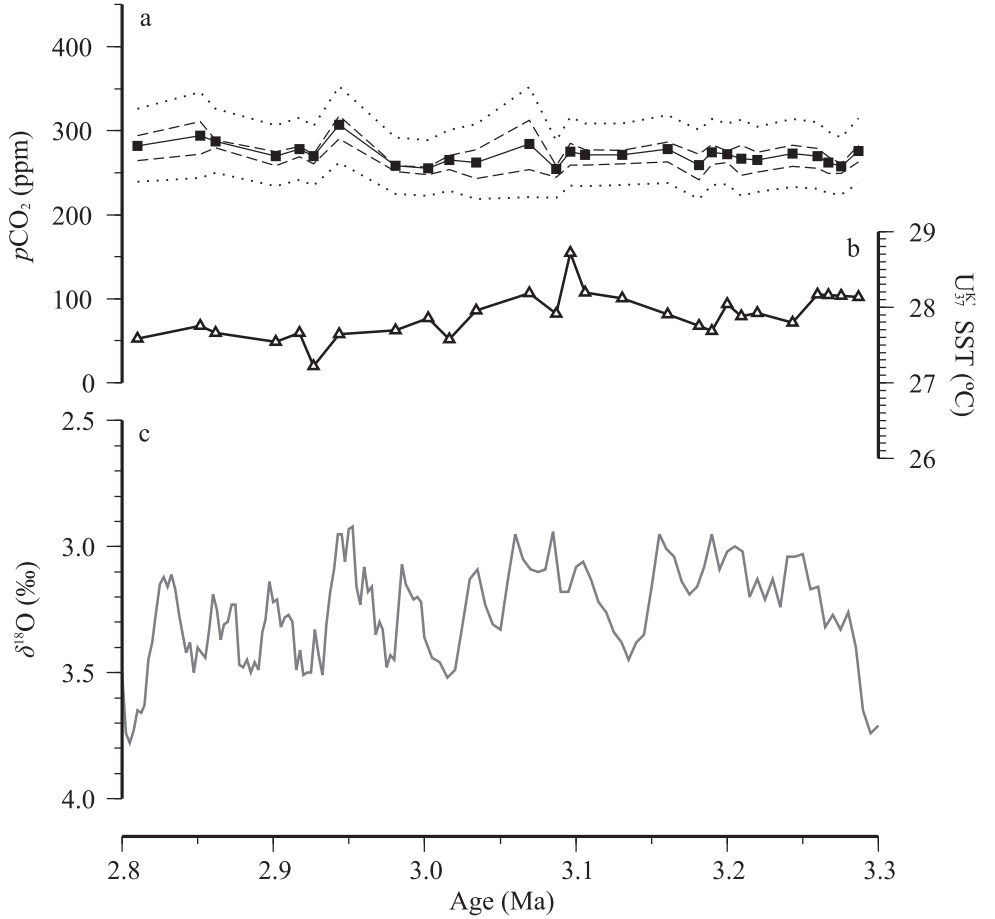

Figure 2a. pCO_2 reconstruction based on our new high resolution $\delta^{13}C_{37:2}$ records (filled squares and line); as in Figure 1, the dashed line shows an uncertainty envelope representing minimum and maximum estimates based on 2σ extremes of the $\delta^{13}C_{37:2}$ measurement (dashed line) and a full monte carlo propagation of associated uncertainties (dotted line; see main text for details). **b**. Sea surface temperature estimates based on the alkenone unsaturation index. Calibration and measurement uncertainties are approximately 2 °C and are omitted for clarity. **c**. Benthic foraminiferal oxygen isotope stack LR04 (Grey/heavy solid line; [9]) for comparison.

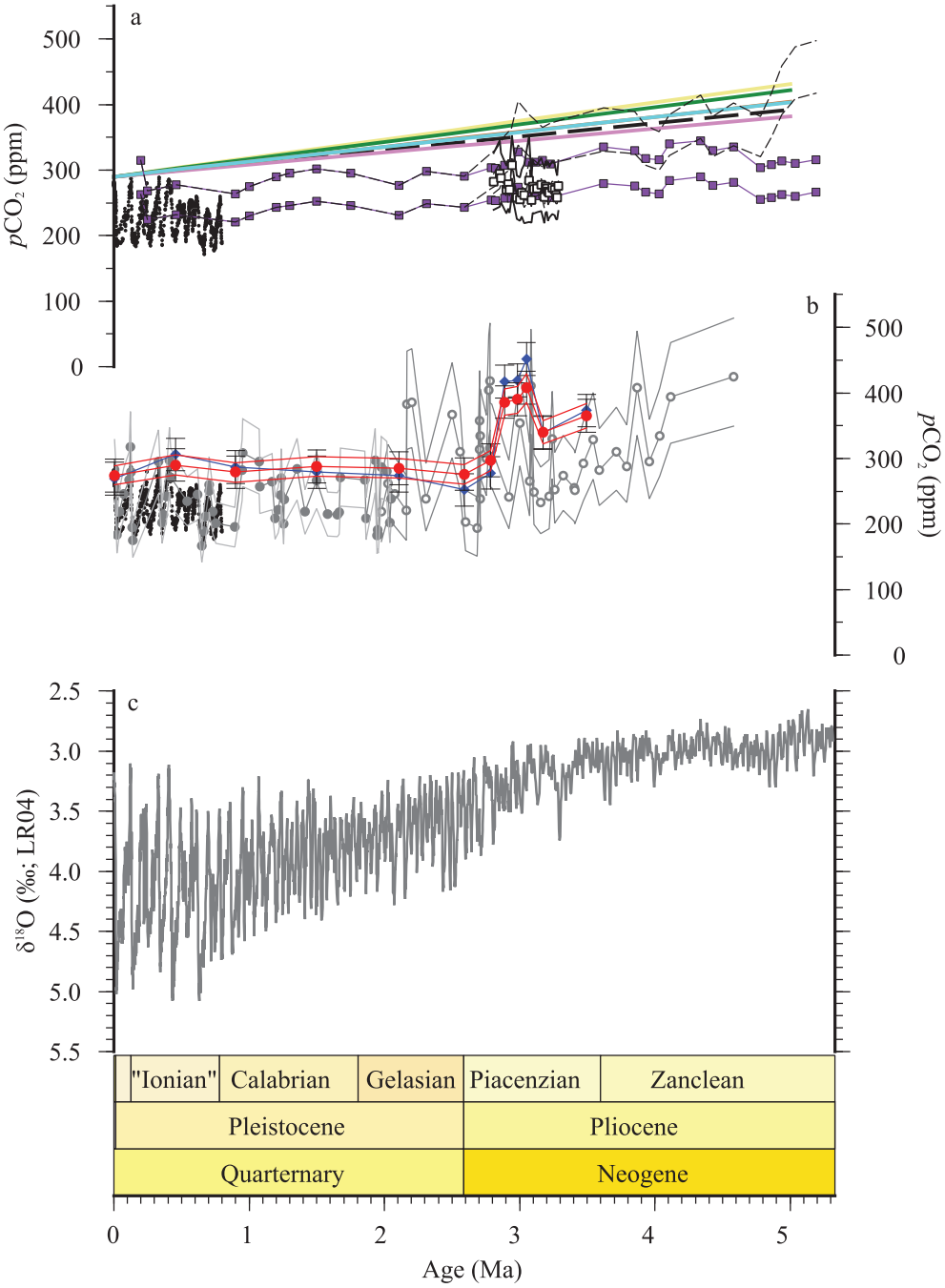

Figure 3 Selected records of pCO_2 and climate from the Pliocene to present. a. Alkenone-based pCO_2 records from Seki et al. [7] corrected for cell geometry (dashed line; minimum and maximum estimates) and uncorrected (purple filled squares and line; minimum and maximum estimates) and Pagani et al. [6] shown here as their reconstructed 'CO_{2slope}' (from top to bottom: from ODP sites 1012 [khaki heavy line]; 1208 [green heavy line]; 982 [cyan heavy line]; 1012 with an alternative nutrient scenario [heavy dashed line]; and 806 [lilac heavy line]. Our record is shown as open squares and line with the error envelope from the monte carlo model (see text). **b**. δ^{11}B-based pCO_2 records from Seki et al. [7] calculated using modelled [CO_3^{2-}] (blue filled diamonds) and assuming modern total alkalinity (TA; red filled circles). Error bars are ±25 ppm and the error envelope is based on varying TA by ±5%. The records of Bartoli et al. [8] are shown in grey, (open grey circles and line, with 2σ uncertainty envelope) along with that of Hönisch et al. [50] (filled grey circles and line, , with 2σ uncertainty envelope). Also shown is the Antarctic ice core record of pCO_2 over the last 800 Kyrs for comparison ([12] and references therein). **c**. Benthic foraminiferal oxygen isotope stack LR04 (Grey/heavy solid line; [9]) for comparison (Online version in colour.)

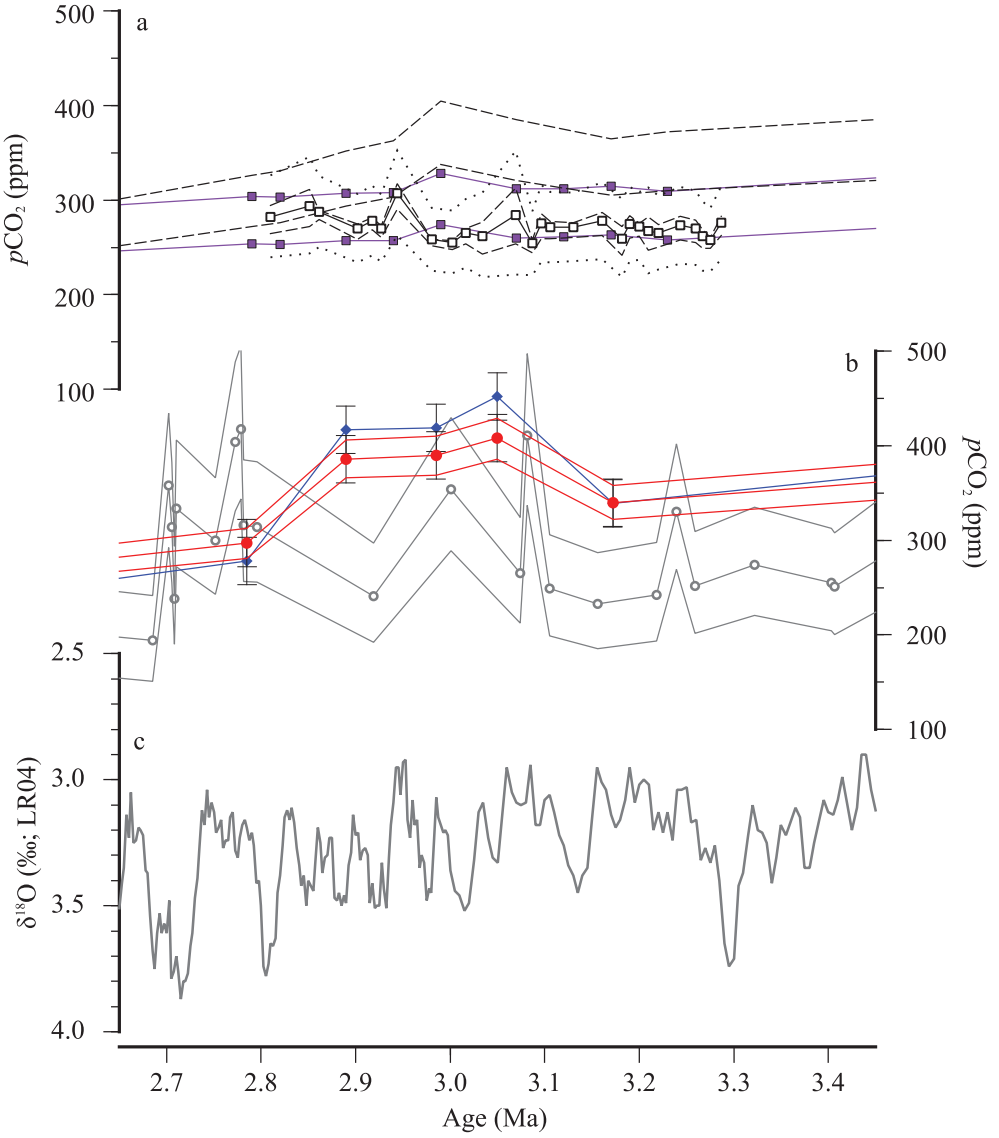

Figure 4. Pliocene pCO_2 records from ODP Site 999. a Alkenone-based pCO_2 records from Seki et al. [7] corrected for cell geometry (dashed line; minimum and maximum estimates) and uncorrected (purple filled squares and line; minimum and maximum estimates) and our new higher resolution record (filled squares and line); the dashed line shows an uncertainty envelope representing minimum and maximum estimates based on 2σ extremes of the $\delta^{13}C_{37:2}$ measurement (dashed line) and a full monte carlo propagation of associated uncertainties (dotted line; see main text for details). b δ^{11}B-based pCO_2 records from Seki et al. [7] calculated using modelled [CO_3^{2-}] (blue filled diamonds) and assuming modern total alkalinity (TA; red filled circles). Error bars are ±25 ppm and the error envelope is based on varying TA by ±5%. The record of Bartoli et al. [8] is shown as grey open circles and line with 2σ uncertainty envelope (grey lines). c. Benthic foraminiferal oxygen isotope stack LR04 (Grey/heavy solid line; [9]) for comparison (Online version in colour.)

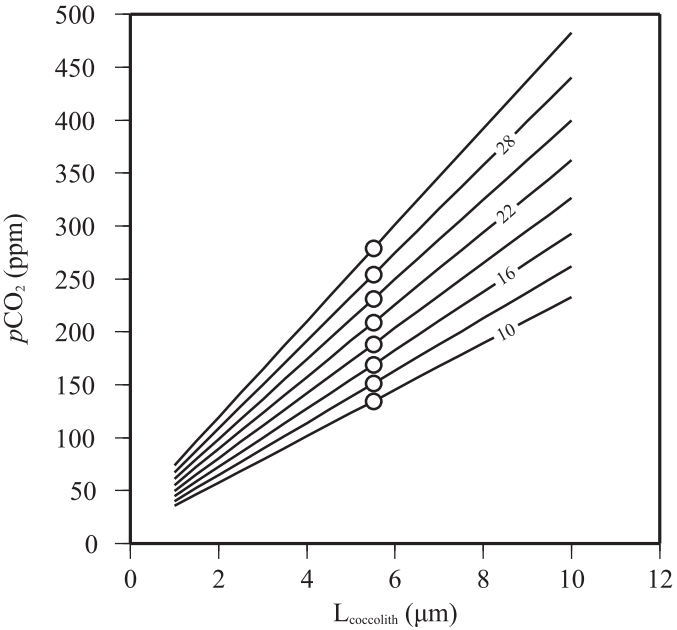

Figure 5 The effect of the coccolith length ($L_{coccolith}$) correction on reconstructed pCO_2. Lines represent the correction applied at different sea surface temperatures at 3 °C intervals (as labelled). White circles represent the uncorrected values (where the coccolith length equals that of modern cultured coccolithophores). These were calculated based on representative values of $\delta^{13}C_{37:2}$= -20 ‰ and $\delta^{13}C_{cc}$= 2 ‰, [PO_4^{3-}]=0.25 μM and S=35 psu.

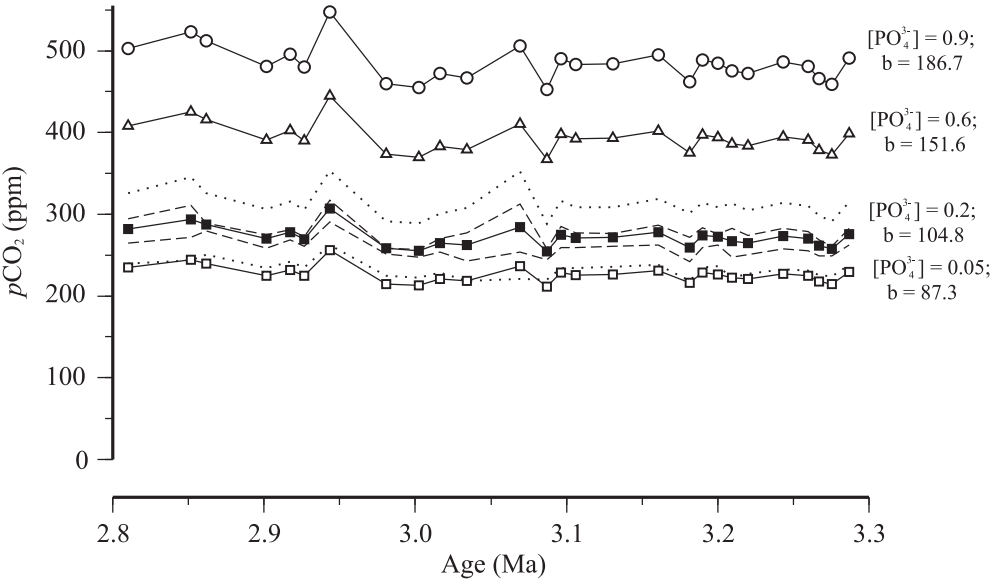

Figure 6 Phosphate concentrations are closely correlated with apparent 'b' term, most likely due to a linkage to growth rate. Our favoured assumption uses the modern day concentration for the site (0.2 μM; black filled squares and line) with minimum and maximum estimates based on 2 σ extremes of the $\delta^{13}C_{37:2}$ measurement (dashed line) and a full monte carlo propagation of associated uncertainties (which includes a ± 0.1 μM on [PO_4^{3-}]; dotted line; see main text for details). We also include reconstructions with [PO_4^{3-}] representative of an oligotrophic site (0.05 μM; open squares), a high nutrient area similar to the eastern equatorial Pacific (0.6 μM; open triangles) and an extreme case representative of an active upwelling region (0.9 μM; open circles)[45]. The appropriate 'b' term according to the relationship of Pagani et al. [6] is shown for each reconstruction.

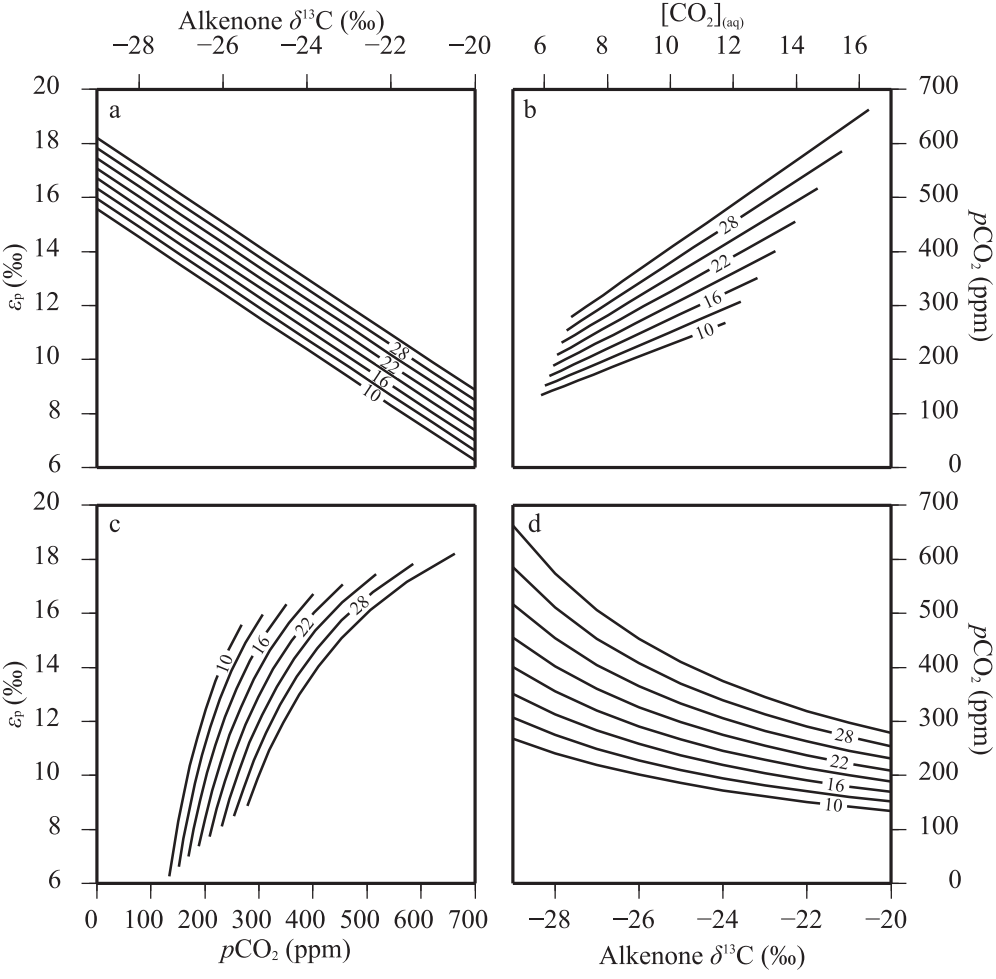

Figure 7 The relationship between ε_p and alkenone δ^{13}C (a); $[CO_{2(aq)}]$ and pCO_2 (b); ε_p and pCO_2 (c); and alkenone and δ^{13}C (d) are all affected by SST. Lines are calculated at varied SST at 3 °C intervals (as labelled), and were calculated based on representative starting values of $\delta^{13}C_{37:2}$= -20 ‰; $\delta^{13}C_{cc}$= 2 ‰. $[PO_4^{3-}]$=0.25 μM, S=35 psu.